



ARTICLE

Experimental and Numerical Study on Progressive Collapse Analysis of a Glulam Frame Structure: I. Side Column Exposed to Fire

Xiaowu Cheng, Xinyan Tao and Lu Wang*

College of Civil Engineering, Nanjing Tech University, Nanjing, 211816, China

*Corresponding Author: Lu Wang. Email: kevinlwang@njtech.edu.cn

Received: 14 April 2022 Accepted: 15 July 2022

ABSTRACT

This paper presents experimental and numerical investigations on progressive collapse behavior of a two-story glulam frame when the side column is exposed to ISO834 standard fire. The collapse mechanism initiated by fire is identified. The experimental results show that the progressive collapse of a glulam frame could be described for three stages, namely bending effect stage, catenary effect stage and failure stage, respectively. These stages are discussed in detail to understand the structural behavior before and during collapse. It is demonstrated that the entire frame slopes towards the side of the heated column, and the “overturning” collapse occurs eventually. The catenary effect of beams is the main reason for the progressive collapse of the frame. In addition, a finite element model of a glulam frame is established to simulate the progressive collapse behavior. The effects of axial loads on the columns are summarized. The numerical simulation results agree well with the experimental results, which could verify the effectiveness and practicability of finite element simulation. Furthermore, the progressive collapse resistance of the frame in practical design were proposed.

KEYWORDS

Collapse; glulam frame structure; fire; failure mechanisms

1 Introduction

The woods are regarded as the green building material. Hence, the glulam frame structures have been extensively used in construction because of their advantages of green, strength and durability, such as stadiums, airports and exhibition halls. However, there are many cases of fire induced progressive collapse in buildings, resulting in great losses. Due to the thermally degradability and combustibility of wood, the cross section and the bearing capacity of the timber components decrease seriously under fire conditions [1–5], leading to the collapse ultimately.

In recent years, considerable interests in the collapse of frame structures subjected to fire have been aroused, and extensive efforts have been devoted to the studies by many professional researchers. Ali et al. [6] simulated the deformations and collapses of single-story bare steel frames under fire. The influences of extent of fire, roof loads and frame dimensions on collapse of single-story frames were also studied. The numerical simulations revealed that the collapse could be toward the firewall. The increase of spatial extent of fire and roof weight accelerated the failure. Agarwal et al. [7] analyzed and evaluated the stability behavior and collapse of ten-story steel building structures subjected to fire. The results



indicated that gravity columns govern the stability of structure in fire conditions. The load generated by the failed column could be redistributed to the neighboring columns to maintain the stability of the whole structure through catenary action. Lange et al. [8] illustrated two different types of collapse mechanism initiated by fire, namely, a weak floor failure mechanism and a strong floor failure mechanism. A design method was proposed which could estimate the potential for collapse of tall buildings in fire. Based on a series of results from the numerical modelling, the methodology presented is conservative. Li et al. [9] simulated the fire-induced collapse of an 8-storey RC-frame-supported masonry building and discussed the primary reasons. The simulation demonstrated that the interior columns were severely damaged, which significantly weakened the bearing capacity of the structure. Failure of the adjacent area may further trigger the progressive collapse. Besides, design suggestions on the key structural components, the fire compartments, and the structural robustness were given to prevent the collapse. Lu et al. [10] established a finite element of a super-tall reinforced concrete building to simulate the mechanical behavior and identify the mechanisms of the fire-induced progressive collapse. The results showed that collapse was triggered by the flexural failure of the peripheral columns which is attributed to the thermal expansion of the floor. Lou et al. [11] recorded the detailed thermal and structural responses of a full-scale 36 m × 12 m steel portal frame under natural fire conditions and investigated the collapse mechanism. The results showed that temperature distribution was non-uniform along the frame height and the temperature gap of lower and upper half region was huge. Outward bending of the column caused by the asymmetrical fire scenario was also found.

Compared with the studies of steel and concrete structures, the researches of the timber structures have more concentrated on the collapse at room temperature [12–22]. Bedon et al. [23] studied the in-plane compressive performance of timber walls under fire through standard fire tests and finite element numerical simulations. The results show that additional insulation on the wall surface can prevent the spread of flames, thereby preventing premature collapse of the structure. Jessop et al. [24] conducted a natural fire test to evaluate the fire resistance of light timber buildings under lateral loads. The results show that after the gypsum board ceiling falls, the lower chord of the roof truss was broken, causing the fire wall to lose lateral stability and the structure progressive collapse. Whelton et al. [25] conducted experimental and numerical studies on the collapse resistance of steel-timber composite structures. The results showed that the fire resistance time of the structure was increased by an average of 34.3% after the reinforcement was implanted in the timber members. Zhang et al. [26] studied the fire test of beam-column wood frame, and showed that the fire cracked at the bottom of the span of the wood frame beam, and the ultimate bearing capacity was significantly reduced. Zhang [27] conducted a fire resistance limit test on the steel-wood bolted timber frame at high temperature. The research shows that reducing the load level of the specimen can effectively improve the fire resistance of the wood frame. However, previous researches have much greater reliance on numerical simulation and experimental results is limited. Therefore, it is necessary to conduct the experimental study on the progressive collapse of glulam frames exposed to fire.

In this paper, a two-story and two-bay glulam plane frame was designed and tested, consisting of columns and beams with wood-steel-wood bolted connections. The temperatures and displacements of different components and connections were measured and compared. Meanwhile, the failure mechanism of glulam frame structure under ISO834 standard curve fire was analyzed and investigated. In addition, a finite element model of glulam frame was established to study the effects of axial loads on the progressive collapse.

2 Materials and Methods

2.1 Design of Frame

In accordance with GB/T 50329-2012 “Standard for test methods of timber structures” [28], GB 55006-2021 “General code for steel structures” [29] and GB 55005-2021 “General code for timber structures”

[30], a 2-storey and two-span plane frame is designed with reference to the actual office building. The scale ratio of the frame is 1:3. The column spacing is 1.42 m and floor height is 0.84 m. Douglas fir lumbers are used as the raw material to make five-layer glulam timber components. The material properties of Douglas fir were listed in Tables 1 and 2. The dimension of the section of beam is 100 mm × 150 mm, and the dimension of column is 150 mm × 150 mm. Wood-steel-wood bolted connections are used in this study, which are made of Q235 steel and 8.8 M10 high strength bolts. The columns are connected to the rigid foundation beam by bolts and T-shape steel plates. Detailed dimension of connections is shown in Fig. 1. The rigid foundation beam adopts I-shape cross section of 200 mm × 200 mm × 8 mm × 12 mm, as shown in Fig. 2. The frame is assembled in the furnace in Nanjing Tech University. The process is shown in Fig. 3.

Table 1: Compressive strength of Douglas Fir

Temperature (°C)	Compressive strength parallel to grain (MPa)	Radial compressive strength (MPa)	Tangential compressive strength (MPa)
20	54.54	5.59	9.42
100	71.42	6.89	10.16
180	58.32	6.40	9.97
250	32.23	3.94	5.21

Table 2: Bending strength of Douglas Fir

Temperature (°C)	Bending strength parallel to grain (MPa)
20	92.12
100	100.62
180	89.67
250	65.23

2.2 Loading Scheme

The fire test was carried out in the furnace of the fire engineering laboratory in Nanjing Tech University. The temperature-time curve in the furnace was consistent with ISO834 standard fire curve. The rock wool was used to wrap the unfired members for fire protection, as shown in Fig. 4. The vertical load was applied to the top of columns by means of hydraulic jacks, so that the effects of the weight of superstructure and pile load on beam could be taken into consideration. Meanwhile, the load was kept at 150 kN by adjusting the oil pump, as shown in Fig. 5.

2.3 Layout of Measurement Points

In this study, XC-K-2 × 0.5 thermocouple manufactured by Nanjing Keiside company was used to measure temperatures in structural components. As shown in Fig. 6, temperature measurement points (T1, T2, T3, T4, T5 and T6) were installed along the height of the heated column with an interval of 50 mm and the buried depth increased successively in 30 mm as a unit. Meanwhile, the thermocouples (T7, T8, T9 and T10) were arranged along the width of the column with an interval of 30 mm and at a distance of 0, 25, 50, 75 mm from the fire-exposed surface. The mid-span temperature of the heated beam was also recorded. The thermocouples (T13, T14, T15 and T16) were placed inside the beam at a distance of 0, 50, 100 and 150 mm from the fire-exposed surface, respectively. Besides, the pull line displacement meter was used to measure the displacement of the members. The detailed layout of measurement points of displacements is shown in Fig. 7.

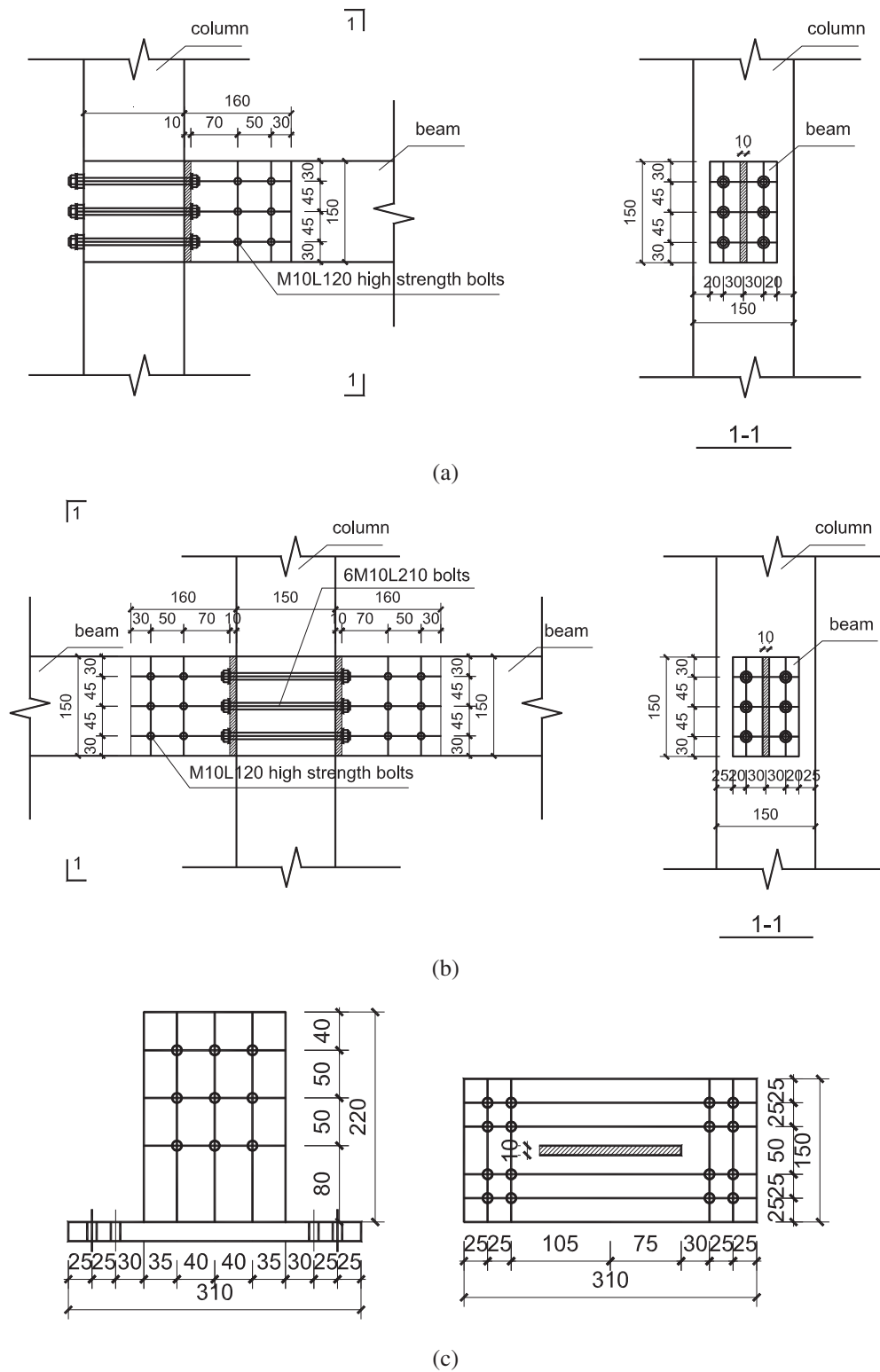


Figure 1: Detailed dimension of connections. (a) Joint connected beam to side column, (b) joint connected beam to central column, (c) joint connected beam-on-foundation to column

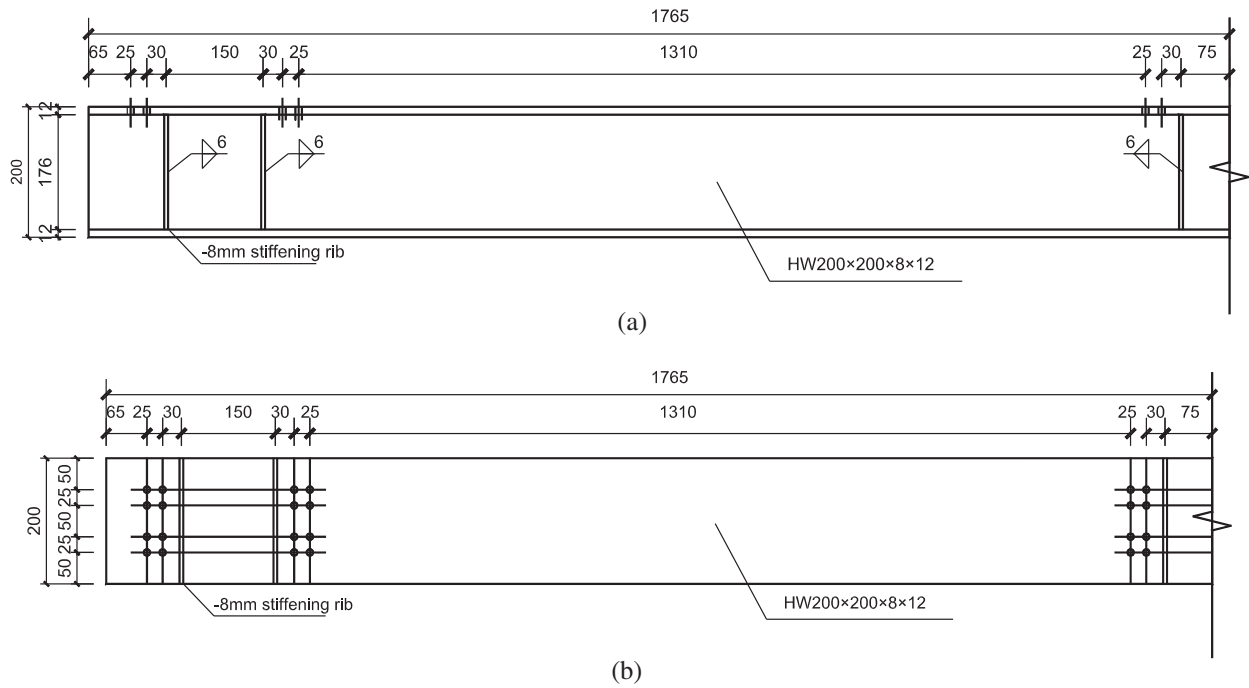


Figure 2: Details of rigid foundation beam. (a) Elevation view, (b) plan view



(a)



(b)

(c)

(d)

Figure 3: Assembly process of the frame. (a) Installation of wood-steel-wood bolted connections, (b) installation of columns, (c) installation of beams, (d) the entire frame

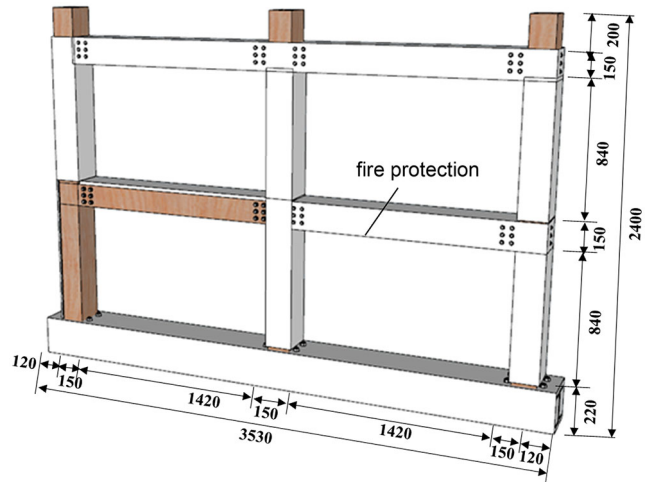
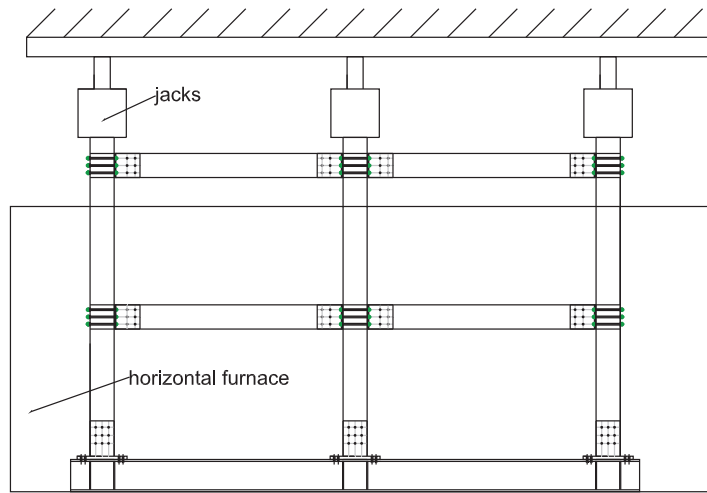


Figure 4: Fire protection of the frame



(a)



(b)



(c)

Figure 5: Loading of the frame. (a) The vertical load, (b) oil pump, (c) jacks

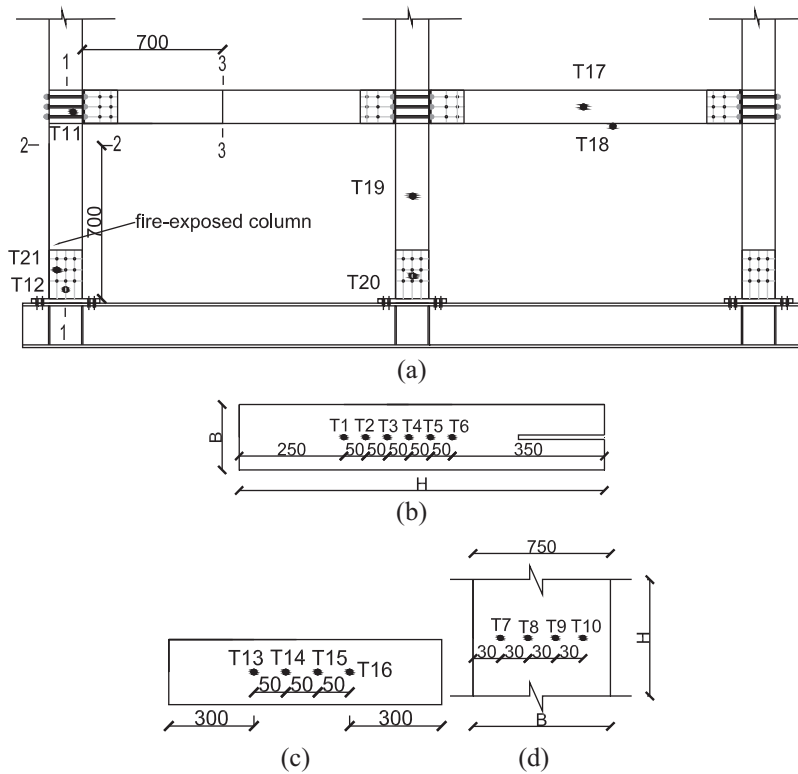


Figure 6: Locations of measurement points of temperatures. (a) Measurement points of the frame, (b) measurement points along the height of the fire-exposed column, (c) measurement points along the width of the fire-exposed column, (d) measurement points of the fire-exposed beam

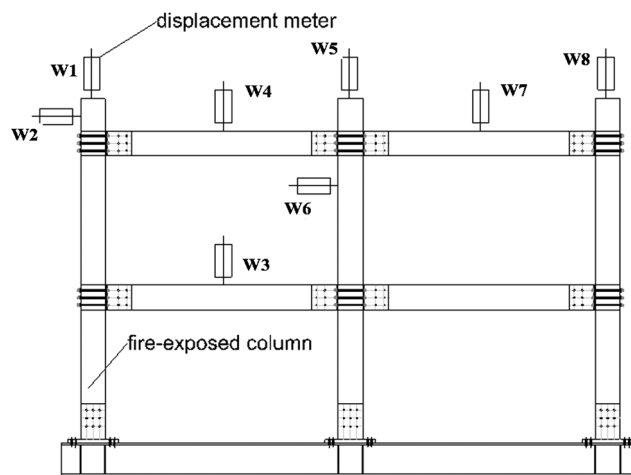


Figure 7: Detailed layout of measurement points of displacements

3 Results and Discussion

3.1 Test Observations

Experimental phenomena at critical time points were observed and recorded. At the 10th minute, the surface of the heated column began to burn completely. The fire entered its fully development period.

Reaching the 26th min of fire exposure, the vertical displacement of the side column increased obviously. As shown in Fig. 8, the out-of-plane displacement of the frame occurred under the bias of the column and the structure was sprayed. The fire was extinguished at the 30th min.



Figure 8: Overall deformation of the frame

3.2 Temperature Distribution

The temperature distributions at different locations of the frame were obtained by using K-type thermocouples. It can be seen from Fig. 9a that the maximum temperatures are 202.5°C, 90.6°C, 76.3°C, 74.8°C, 124.7°C and 838.9°C, respectively, when the buried depths of thermocouples are corresponding 0, 30, 60, 90, 120 and 150 mm. The measured temperature-time curve of the exposed surface was approximately consistent with ISO834 standard fire curve. Because the fireproof cotton did not play a complete insulation effect, the unexposed surface has higher temperature than that inside the heated column. The temperature at 120 mm depth of the backfire surface is higher than that at 90 mm depth, which is caused by the increase of the depth of the carbonized layer.

As shown in Fig. 9b, it can be found that the temperature of fire-exposed surface increased following the development of the temperature in the furnace. The location at a distance of 25 mm beyond the fire-exposed surface was heated up to 439.8°C. For deeper locations (50 and 75 mm), the temperature increased over 90°C. The maximum temperature value decreased with the increase of buried depth of thermocouples.

Fig. 9c shows the temperature-time curves of the components and connections under fire protection. It can be seen that the measured highest temperature occurred at the foot of the fire-exposed column. The wood-steel-wood bolted connection, which was close to the heated column, had an obvious increase in temperature on account of the heat transferred from the column. In the meantime, the components did not achieve the level of fire-resistance required with the use of fireproof cotton, resulting in a slight rise in temperature.

The locations, where were 0, 50, 100, 150 mm away from the unexposed surface, reached its peak temperature of 218.3°C, 86.2°C, 113.7°C, 826.5°C within 30 min, as shown in Fig. 9d. The fire exposed surface had a similar temperature time history to ISO834 standard fire. Due to the defects of artificial fire protection, the unexposed surface had an obviously higher temperature than inside the heated beam. The location at a distance of 100 mm beyond unexposed surface was about 700°C, which was lower than the exposed surface because of the carbonized layer.

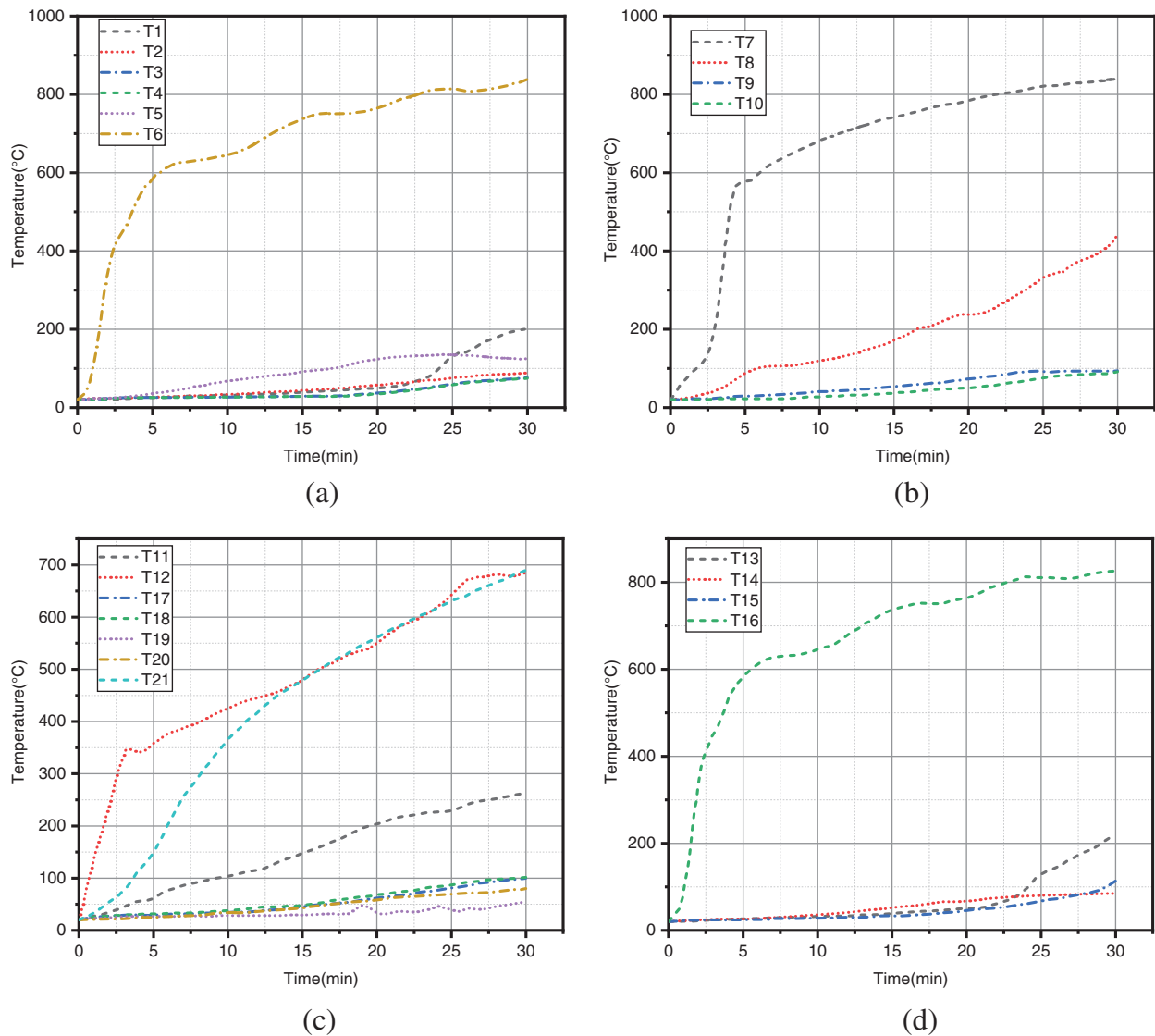


Figure 9: Temperature-time curves of the frame. (a) Temperature distribution along the height of the heated column, (b) temperature distribution along the width of the heated column, (c) temperature distribution of components and connections under fire protection, (d) temperature distribution of the heated beam

3.3 Displacement

During the tests, the displacement of columns and beams were monitored. The relationship between temperature and displacement was obtained. When the fire extinguished, the frame was also monitored to analyze the displacement in the cooling stage. According to the layout direction of the displacement meter, the measured displacement was the increase of the length along the pulling direction of the displacement meter.

The displacement-temperature curves of the heated column are presented in Fig. 10a. The W1 was the vertical displacement of the column subjected to fire, while W2 was the lateral displacement of the column subjected to fire. With the temperature reaching 700°C, the displacement began to increase rapidly. When the temperature was above 800°C, the displacements at horizontal and vertical directions reached the maximum

values. It can be found that the maximum vertical displacement was 96.56 mm, and the maximum lateral displacement was 15.1 mm. The slight fluctuation may be caused by the expansion and contraction of the component.

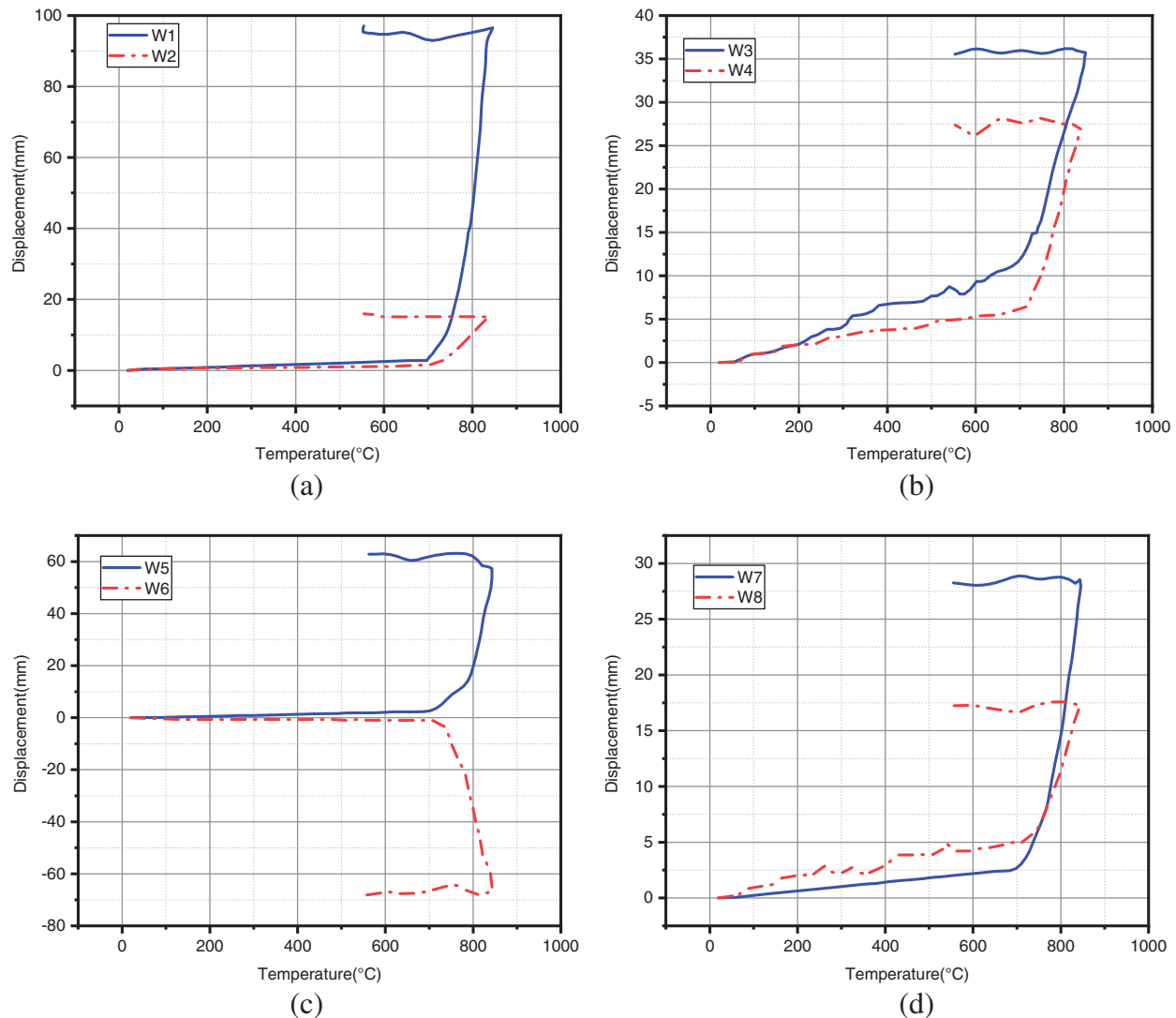


Figure 10: Displacement-temperature curves of the frame. (a) Vertical and lateral displacement of the heated column, (b) mid-span displacement of beams, (c) vertical and lateral displacement of the central column, (d) displacement of unexposed components

The mid-span displacement of the beams was close to the heated column as shown in Fig. 10b. The W3 was the mid-span displacement of the first level beam and W4 was the mid-span displacement of the second level beam. The growth rate of displacement of the first level beam was basically consistent with that of the second level beam at the initial stage of the test. However, the section of the first level beam was weakened with the increase in temperature, as it can account for a rapid displacement rise. Meanwhile, the growth rate of the mid-span displacement of the first level beam was gradually greater than that of the second level beam because of the downward movement of the heated column. It can be found that the displacement of the first level beam reached its maximum value of 35.72 mm and the

displacement of the second level beam reached its maximum value of 27.43 mm. Due to the continuous weakening of the cross section, the failure of the heated beam was priority over the connections.

Fig. 10c plots the displacement-temperature curves of the central column. The W5 represented the vertical displacement of the central column, while W6 represented the lateral displacement of the central column. It is demonstrated that the central column sloped toward the side of the heated column due to the large deflection of the connecting beam with a critical temperature of about 700°C. As shown in Fig. 11, the maximum displacement of the central column reached 57.26 mm and the lateral displacement of the central column reached 66.89 mm, respectively. Subsequently, the connections of the central column were deformed and destroyed, and the central column was a tendency of collapse.

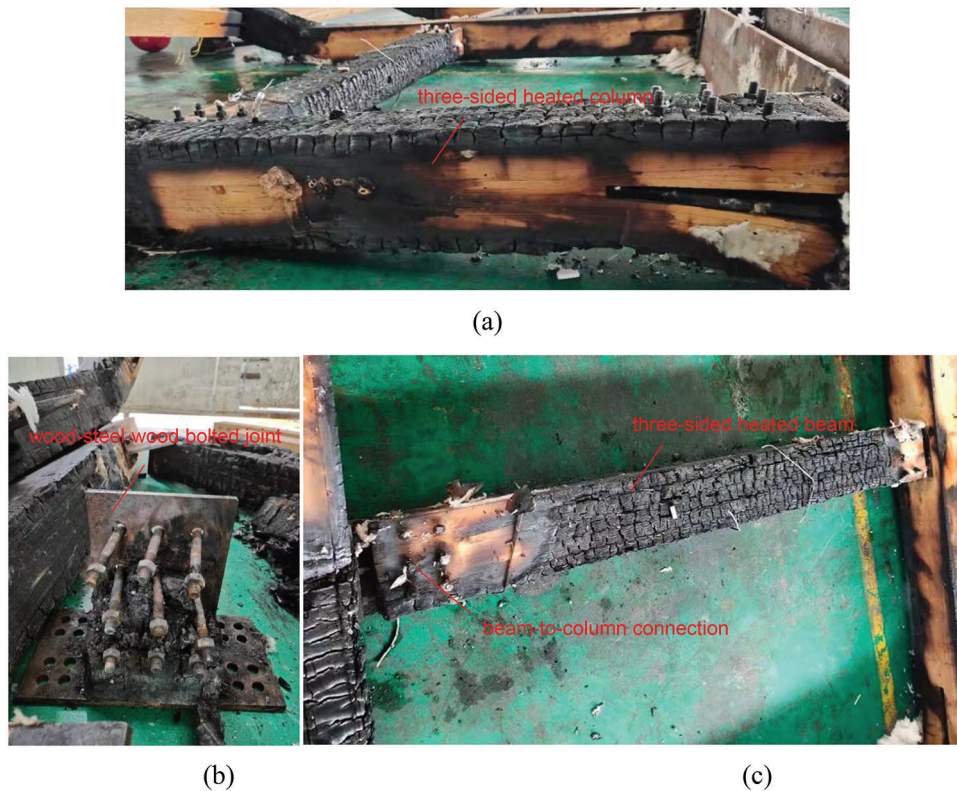


Figure 11: The failure mode of the frame. (a) The three-sided heated column, (b) wood-steel-wood bolted joint connected beam-on-foundation to the heated column, (c) the three-sided heated beam

Fig. 10d shows that the displacement of the unexposed components, where W7 represented the mid-span displacement of the second layer beam and W8 represented the vertical displacement of the side column. It can be found that the maximum mid-span displacement of the beam was 28.56 mm and the maximum vertical displacement of the column was 17.32 mm, respectively. The maximum value was smaller than that of the members which were close to the fire. The results showed that the fire-induced progressive collapse effect of the frame was reduced due to the force sharing of the central column and beams.

3.4 Failure Mode and Mechanism

The frame experienced significant deformation and destruction at elevated temperatures. The failure mode of the three-sided heated column is shown in Fig. 11a, and the failure mode of wood-steel-wood bolted connection at the foot of the heated column is presented in Fig. 11b. The fire exposed column was

mainly vertical buckling failure, eventually resulting in cracking at the bottom of the unexposed surface. It also illustrates that the overall deformation of the frame was partly attributed to the destruction of the connections. As shown in Fig. 11c, the section of the three-sided heated beam severely weakened, which derived the beam to bend ultimately. In the meantime, the beam-to-column connection seriously deformed due to the buckling of the heated column and large deflection of the heated beam, which showed good agreements with the phenomenon in actual cases.

Failure initiated in the side column subjected to fire and spread progressively to adjacent beams. It is demonstrated that the weakening of the section of the fire-damaged column contributed to the buckling and vertical and lateral displacements. Simultaneously, the joint connecting the beam and the heated column was angular deformation. With fire-exposed time extending, the lateral displacement of the central column become larger due to catenary forces and the shear failure of the joints. Therefore, the frame gradually trended to overturn and collapse towards the side of the heated column. Later, the beam far away from the heated column showed slight deflection. The unexposed side column showed slight vertical displacement. Ultimately, the frame had a tendency of progressive collapse.

The characteristics of the frame during the progressive collapse were obtained and the different failure mechanisms were analyzed. Hence, the test could be described by use of three stages, which were bending effect stage, catenary effect stage and failure stage, respectively. According to the displacement-temperature curves of the heated column and the central column, it can be found that the entire frame was in the elastic-plastic deformation stage where the displacement of components were slight before the temperature of the fire-exposed surface reaches 700°C. At this stable stage, the frame met all kinds of calculation criteria of statically indeterminate structure and there is no change of bending moment and shear force inside the structure.

When the temperature was over 700°C, the displacement of the members increased rapidly and then the frame can be considered to enter the catenary effect stage. The displacement of the entire frame in the catenary effect stage is shown in Fig. 12. When the vertical displacement of the heated column reached 96.56 mm, the mid-span displacement of the second layer beam was 27.43 mm and the lateral displacement of the adjacent central column reached 66.89 mm, as shown from the displacement-temperature curves. Under the combined action of the flexural properties of the beam and the shear properties of the connection, the central column was obvious lateral displacement and tended to overturn towards the side of the heated column. Therefore, in order to prevent the toppling collapse initiated by the destruction of the side column, the catenary effect of the beam should be minimized.

When the frame reaches the final failure stage, the catenary action of the beam fails and the beam-to-column connections quit the work completely. The destruction of the central column drives the frame collapse. If the test continues, the central column will gradually withdraw from the work and the unexposed column will be destroyed under the catenary effect of the adjacent beam. Eventually, the entire frame will completely collapse.

3.5 Numerical Simulation

A finite element model of the glulam frame was established in ABAQUS. The simulation results at the initial stage of catenary effect were compared with the experimental results to verify the effectiveness and practicability of finite element simulation of progressive collapse of timber frame under fire conditions. The model consisted of two types of elements: eight-node linear brick (C3D8R) for stress control, and eight-node linear heat transfer brick (DC3D8R) for heat transfer. The boundary condition of bottom column ends were fixed support. The C3D8R element considered the anisotropic mechanical properties, including the Young's modulus, shear modulus and Poisson's ratio of wood along the longitudinal, radial, and tangential axes. Because the compressive behavior of the columns was mostly dominated by the

parallel to grain stress–strain relationship, the mean values of the test results were discretized to establish a ABAQUS input stress–strain table for the FEM model.

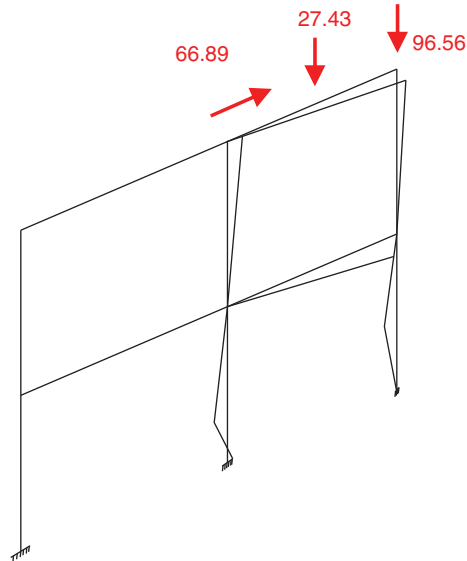


Figure 12: The displacement of the entire frame

As shown in Fig. 13, the deformation cloud diagram of the frame at the 25th minute was obtained according to the results of thermo-mechanical coupling. It can be found that the wood-steel-wood bolted connection at the foot of the fire-exposed column was preferentially compressed and failed. In the meantime, the vertical displacement of the fire-exposed column and the bending of the adjacent beam occurred, which derived the lateral displacement of the central column finally. This was consistent with the initial destruction of the frame during the test.

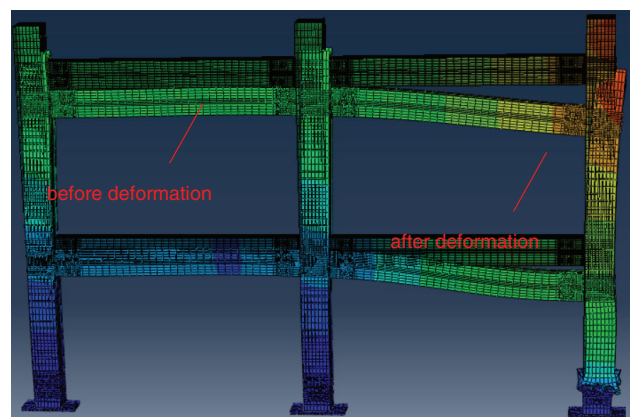


Figure 13: The simulation deformation of the entire frame

The simulated values of vertical and lateral displacement of the fire-exposed column were compared with the experimental values, as shown in Fig. 14. It is demonstrated that the trend of measured displacements and simulated displacements of timber frame structure at the initial stage of collapse were basically the same. A slight inconsistency may be attributed to the unstable performance of jacks and oil

pump in the process of loading. In general, the thermodynamic coupling model can effectively simulate the real deformation of the frame in the tests, which could provide reference for design.

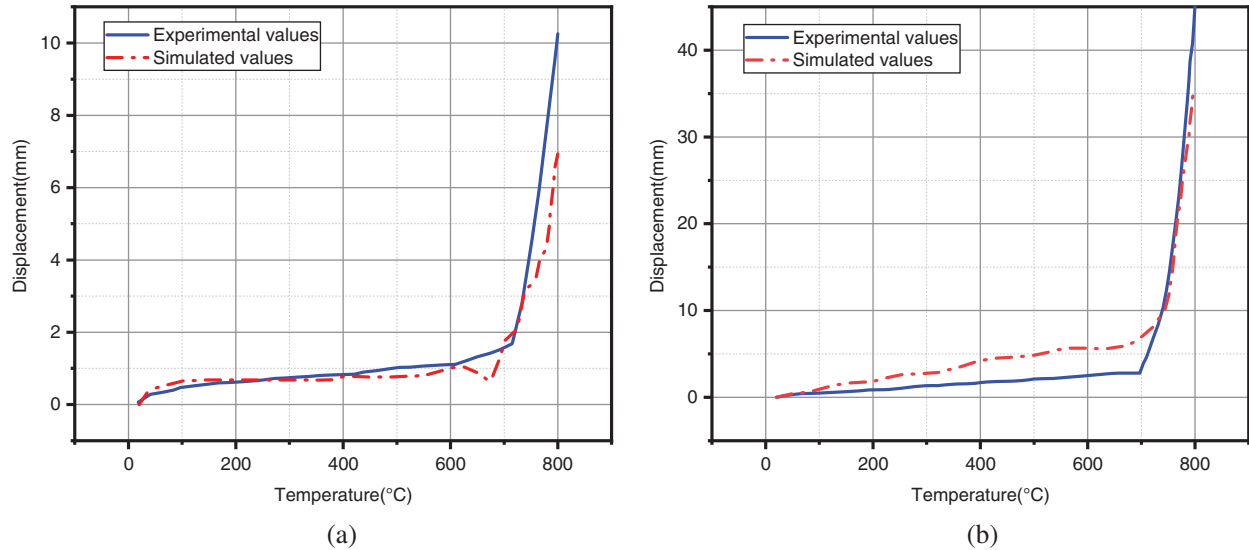


Figure 14: Comparison between experimental values and simulated values of the fire-exposed column. (a) Vertical displacement, (b) lateral displacement

Due to the limitation of test conditions, the axial force of the column subjected to fire is not measured in the test. In order to further improve the theoretical analysis of fire-induced progressive collapse, the curve of the axial force time is plotted in Fig. 15 according to numerical simulation results. It can be seen that the axial force of the heated column began to drop significantly at the 25th min when the vertical displacement of the column began to increase significantly. At this time, the temperature in the furnace reached about 800°C.

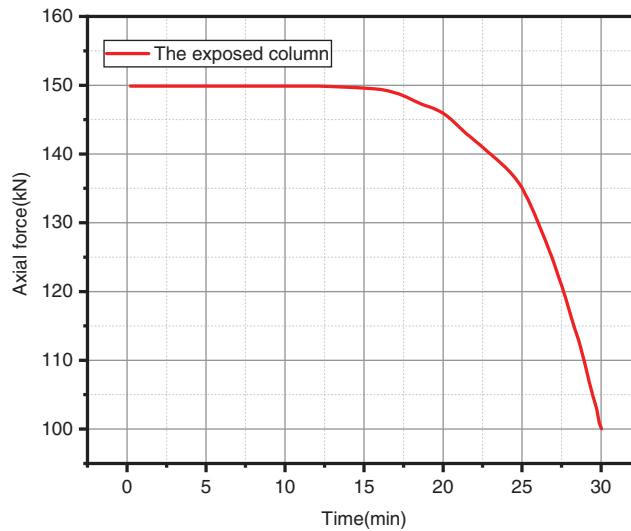


Figure 15: The axial force of the fire-exposed column

4 Conclusions

In this study, the test on collapse resistance of side columns of glulam frame structure under fire was conducted. Based on the experimental work and analytical results, the following conclusions can be drawn.

1. The vertical displacement of the heated column appears after 18 min fire exposure, which is caused by the weakening of cross section. The height of the fire column decreases obviously after being exposed to fire for 25 min. Meanwhile, the lateral displacement of the central column appears due to the flexural failure of the beam.
2. Events leading up to the progressive collapse of glulam frame could be described for three stages that are bending effect stage, catenary effect stage and failure stage. The frame tends to slope towards the side of the heated column and the overturning collapse occurs ultimately.
3. The catenary effect of the beam is the main reason for the collapse of the glulam frame structure initiated by fire. In order to improve the ability to resist collapse, the compressive strength of the central column should be improved.

Acknowledgement: The authors express many thanks to Nanjing Gongda Construction Technology Co., Ltd.

Funding Statement: This research was funded by the Jiangsu Province Science Fund for Distinguished Young Scholars (Grant No. BK20211536) and Research Foundation of Nanjing Gongda Construction Technology Co., Ltd. (Grant No. 2021RD01).

Conflicts of Interest: The authors declare that they have no conflicts of interest to report regarding the present study.

References

1. Schmid, J., König, J., Just, A. (2018). The reduced cross-section method for the design of timber structures exposed to fire—Background, limitations and new developments. *Structural Engineering International*, 22(4), 514–522. DOI 10.2749/101686612X13363929517578.
2. Zhang, Y. W., Wang, L., Chen, L. (2021). Energy-based time equivalent approach for evaluating the fire resistance of timber components exposed to realistic design fire curves. *The Structural Design of Tall and Special Buildings*, 30(11), e1861. DOI 10.1002/tal.1861.
3. Zhang, Y. W., Wang, L. (2021). Research on flashover prediction method of large-space timber structures in a fire. *Materials*, 14(19), 5515. DOI 10.3390/ma14195515.
4. Wang, L., Zhang, Y. W., Ho, J. C. M., Lai, M. H. (2020). Fatigue behaviour of composite sandwich beams strengthened with GFRP stiffeners. *Engineering Structures*, 214(1), 110596. DOI 10.1016/j.engstruct.2020.110596.
5. Schnabl, S., Turk, G., Planinc, I. (2011). Buckling of timber columns exposed to fire. *Fire Safety Journal*, 46(7), 431–439. DOI 10.1016/j.firesaf.2011.07.003.
6. Ali, H. M., Senseny, P. E., Alpert, R. L. (2003). Lateral displacement and collapse of single-story steel frames in uncontrolled fires. *Engineering Structures*, 26(5), 593–607. DOI 10.1016/j.engstruct.2003.12.007.
7. Agarwal, A., Varma, A. H. (2014). Fire induced progressive collapse of steel building structures: The role of interior gravity columns. *Engineering Structures*, 58, 129–140. DOI 10.1016/j.engstruct.2013.09.020.
8. Lange, D., Röben, C., Usmani, A. (2012). Tall building collapse mechanisms initiated by fire: Mechanisms and design methodology. *Engineering Structures*, 36, 90–103. DOI 10.1016/j.engstruct.2011.10.003.
9. Li, Y., Lu, X., Guan, H., Ying, M., Yan, W. (2016). A case study on a fire-induced collapse accident of a reinforced concrete frame-supported masonry structure. *Fire Technology*, 52(3), 707–729. DOI 10.1007/s10694-015-0491-0.
10. Lu, X., Li, Y., Guan, H., Ying, M. (2017). Progressive collapse analysis of a typical super-tall reinforced concrete frame-core tube building exposed to extreme fires. *Fire Technology*, 53(1), 107–133. DOI 10.1007/s10694-016-0566-6.
11. Lou, G., Wang, C., Jiang, J., Jiang, Y., Wang, L. et al. (2018). Fire tests on full-scale steel portal frames against progressive collapse. *Journal of Constructional Steel Research*, 145(4), 137–152. DOI 10.1016/j.jcsr.2018.02.024.

12. Sun, G. J., Wang, C. T., Wang, L. (2022). Study on the fire behavior of sandwich wall panels with GFRP skins and a wood-web core. *Journal of Renewable Materials*, 10(6), 1537–1553. DOI 10.32604/jrm.2022.018598.
13. Gupta, V., Osorio, A. F., Torero, J., Hidalgo, J. P. (2020). Mechanisms of flame spread and burnout in large enclosure fires. *Proceedings of the Combustion Institute*, 38(3), 4525–4533. DOI 10.1016/j.proci.2020.07.074.
14. Wang, L., Sun, J., Ding, T., Liang, Y., Ho, J. C. M. et al. (2022). Manufacture and behaviour of innovative 3D printed auxetic composite panels subjected to low-velocity impact load. *Structures*, 38, 910–933.
15. Munjiza, A., Bangash, T., John, N. W. M. (2004). The combined finite-discrete element method for structural failure and collapse. *Engineering Fracture Mechanics*, 71(4), 469–483. DOI 10.1016/S0013-7944(03)00044-4.
16. Östman, B., Brandon, D., Frantzich, H. (2017). Fire safety engineering in timber buildings. *Fire Safety Journal*, 91(1), 11–20. DOI 10.1016/j.firesaf.2017.05.002.
17. Barber, D., Gerard, R. (2015). Summary of the fire protection foundation report-fire safety challenges of tall wood buildings. *Fire Science Reviews*, 4(1), 1–15. DOI 10.1186/s40038-015-0009-3.
18. Lei, T., Zhang, Y. W., Kuang, D. L., Yang, Y. R. (2019). Preparation and properties of rubber blends for high-damping-isolation bearings. *Polymers*, 11(8), 1374. DOI 10.3390/polym11081374.
19. Grantham, R., Enjily, V. (2004). UK design guidance for multi-storey timber frame buildings. *Proceedings of the 8th World Conference on Timber Engineering*, pp. 19–23. Lahti, Finland.
20. Montalvá, J. M., Osorio, A. F., Torero, J. L. (2019). The Malveira fire test: Full-scale demonstration of fire modes in open-plan compartments. *Fire Safety Journal*, 108(1), 102827. DOI 10.1016/j.firesaf.2019.102827.
21. Yuen, A. C. Y., Chen, T. B. Y., Yeoh, G. H., Yang, W., Cheung, S. C. P. et al. (2018). Establishing pyrolysis kinetics for the modelling of the flammability and burning characteristics of solid combustible materials. *Journal of Fire Sciences*, 36(6), 494–517. DOI 10.1177/0734904118800907.
22. Yuen, A. C. Y., Chen, T. B. Y., Wang, C., Wei, W., Kabir, I. et al. (2020). Utilising genetic algorithm to optimise pyrolysis kinetics for fire modelling and characterisation of chitosan/graphene oxide polyurethane composites. *Composites Part B: Engineering*, 182(1), 107619. DOI 10.1016/j.compositesb.2019.107619.
23. Bedon, C., Fragiacomio, M. (2019). Fire resistance of thermally insulated log-house timber walls. *Fire Technology*, 55(1), 307–341.
24. Jessop, D., Abu, A., Wade, C., Spearpoint, M., Gerlich, H. (2019). Performance of a light timber-framed compartment in natural fire subjected to lateral load. *Fire and Materials*, 43(2), 175–188. DOI 10.1002/fam.2684.
25. Whelton, M., Macilwraith, A. (2017). Timber/steel composite members in multi-storey buildings under fire test loadings. *Journal of Structural Integrity and Maintenance*, 2(3), 152–167. DOI 10.1080/24705314.2017.1354153.
26. Zhang, J., Liao, J., Xu, Q., Zhang, M. (2017). Research on residual bearing capacity of post-beam timber frame after exposure to fire using non-destructive testing. *China Civil Engineering Journal*, 50(11), 45–56 (in Chinese).
27. Zhang, Y. Y. (2016). *Experimental study on the fire performance of post-and-beam timber structure with bolted steel-to timber connection*, pp. 57–88 (in Chinese). Nanjing: Southeast University.
28. GB/T 50329 (2012). *Standard for test methods of timber structures*. Beijing, China: China Building Industry Press.
29. GB 55006 (2021). *General code for steel structures*. Beijing, China: China Building Industry Press.
30. GB 55005 (2021). *General code for timber structures*. Beijing, China: China Building Industry Press.